heritage

MDPI

Article

Comparison of Hyperspectral Imaging and Fiber-Optic Reflectance Spectroscopy for Reflectance and Transmittance Measurements of Colored Glass

Agnese Babini *, Phil Green, Sony George and Jon Yngve Hardeberg

Department of Computer Science, Norwegian University of Science and Technology, 2815 Gjøvik, Norway; philip.green@ntnu.no (P.G.); sony.george@ntnu.no (S.G.); jon.hardeberg@ntnu.no (J.Y.H.)
* Correspondence: agnese.babini@ntnu.no

Abstract: The work presented in this paper is part of a wider research project, which aims at documenting and analyzing stained glass windows by means of hyperspectral imaging. This technique shares some similarities with UV-VIS-IR spectroscopy, as they both provide spectral information; however, spectral imaging has the additional advantage of providing spatial information, since a spectrum can be collected in each pixel of the image. Compared to UV-VIS-IR spectroscopy, spectral imaging has rarely been used for the investigation of stained glass windows. One of the objectives of this paper is, thus, to compare the performance of these two instruments to validate the results of hyperspectral imaging. The second objective is to evaluate the potential of analyzing colored-glass pieces in reflectance modality and compare the results with those obtained in transmittance, in order to highlight the differences and similarities between the two approaches. The geometry of the systems and the backing material for the glass, as well as the characteristics of the glass pieces, are discussed. L*a*b* values obtained from the spectra, as well as the calculated color difference ΔE_{00}, are provided, to show the degree of agreement between the instruments and the two measurement modalities.

Keywords: stained glass; UV-VIS spectroscopy; hyperspectral imaging; colorimetry; transmittance measurements; reflectance measurements

Citation: Babini, A.; Green, P.; George, S.; Hardeberg, J.Y. Comparison of Hyperspectral Imaging and Fiber-Optic Reflectance Spectroscopy for Reflectance and Transmittance Measurements of Colored Glass. *Heritage* **2022**, *5*, 1401–1418. https://doi.org/10.3390/heritage5030073

Academic Editors: Marcia Vilarigues, Sophie Wolf and Teresa Palomar

Received: 11 May 2022
Accepted: 21 June 2022
Published: 23 June 2022

1. Introduction

The work presented in this paper has been carried out within a wider research project [1], which aims at documenting and analyzing stained-glass windows by means of hyperspectral imaging. Hyperspectral imaging (HSI) can be considered as a combination of conventional imaging and UV-VIS-NIR spectroscopy. The technique is based on the acquisition of many images finely sampled across a portion of the electromagnetic spectrum, and, as a result, a full spectrum can be obtained in each pixel of the image, providing information on the materials used as well as their distribution across the artwork under study.

UV-VIS-IR spectroscopy is a well-established technique for the identification of the coloring agents (chromophores) in stained glass windows, whereby the specific absorbance peaks in the spectra can be analyzed and interpreted [2–23]. This information allows for understanding the mechanisms responsible for the color of the glass, which can provide important insights into the technological development in glass production during a particular historical period or geographical region. The use of hyperspectral imaging, on the other hand, is quite limited, and very few works have been published so far on the topic, especially in comparison to the literature available for other typologies of artworks, such as painting and manuscripts [24–27]. Since stained glass is transparent, one of the main practical challenges is to have access to setups that can measure in transmittance. In addition, the setup should be easily, as stained glass windows are usually located in buildings and can be difficult to access without scaffoldings or other supports. The easiest solution, and the most widely used [25–27], is to perform the acquisition by exploiting

solar radiation as light source. However, variations of light distribution throughout the day, as well as the presence of external structures (vegetation, buildings, etc.) might affect the spectra.

Nonetheless, the possibility of having simultaneous spatial and spectral information in HSI can represent a great advantage when analyzing large surfaces such as stained glass windows, compared to spot measurement. In light of these considerations, we recently presented a laboratory setup to perform transmittance hyperspectral imaging of stained glass panels [28].

It is important to highlight that while the detector technologies of HSI and UV-VIS spectroscopy are essentially the same, the two instruments have different optical configuration (array vs. spot measurement) and measurement geometry. One of the objectives of this study is, thus, to evaluate the use of HSI for the analysis of stained glass windows by comparing the results obtained with this technique to those from UV-VIS spectroscopy, following standard geometric recommendations for measurement in transmittance [29–31]. Note that the results from the HSI will be considered only from the spectral point of view, while the spatial dimension will not be taken into account.

Another aim of the paper is to compare the results of two different acquisition modalities: transmittance and reflectance. Traditionally, color measurements of glass are carried out in transmittance mode [30]. Measurements in reflectance are less common; nonetheless, they can be helpful in revealing some properties of the glass under study. In this case, a non-spectrally selective, diffusing surface with high reflectance can be used as a backing material to enhance the reflectance signal of the glass pieces [24,31].

Depending on the transparency of the glass and the surface characteristics, the differences between the results in the two modalities could be interpreted as effects of the surface condition of the colored glass, as can their optical properties.

In this paper, 14 pieces of colored glass have been used as a case study. To compare the results, the geometry of the systems, the characteristics of the glass pieces, and the effects of the backing material for the reflectance measurements will be discussed. The spectra obtained in reflectance and transmittance will be shown together, to visualize the differences in shape and intensity between the two modalities.

CIELAB L*a*b* values and the color difference ΔE_{00}, between the two modalities and the two instruments will be provided for the selected glasses, to show the degree of agreement.

2. Materials and Methods

2.1. Glass Samples

For the experiment, 14 pieces of colored glass, provided by the restoration workshop of the Nidaros Cathedral (Trondheim, Norway), were used (Figure 1). Glass pieces were preferred to real case studies, to facilitate the measurement of transmittance and reflectance as well as the comparison of the instrument configurations.

The glass pieces are modern glass used for restoration purposes, characterized by different thicknesses and surface roughnesses, which strongly influence the intensity and quality of the signals obtained. All the glass pieces are colored in body, except for the red ones; these latter samples consist of two layers, a thinner red layer over a thicker transparent one, consistent with the recipes to create red-colored glass in antiquity.

2.2. Instrumentation

2.2.1. Metrology

The measurements were made using two instruments, a spectrometer and a hyperspectral camera. The Ocean Optic USB2000+ spectrometer (denoted FORS below), is equipped with a fiber-optic connector between the measurement probe and the spectrometer entrance port, with a diffuser mounted over the probe. The hyperspectral camera used for the study was a HySpex VNIR-1800, developed by Norsk Elektro Optikk AS. Figure 2 shows the

respective geometries of the two instruments and the measurement modalities employed, while Table 1 reports the specifications of the instruments.

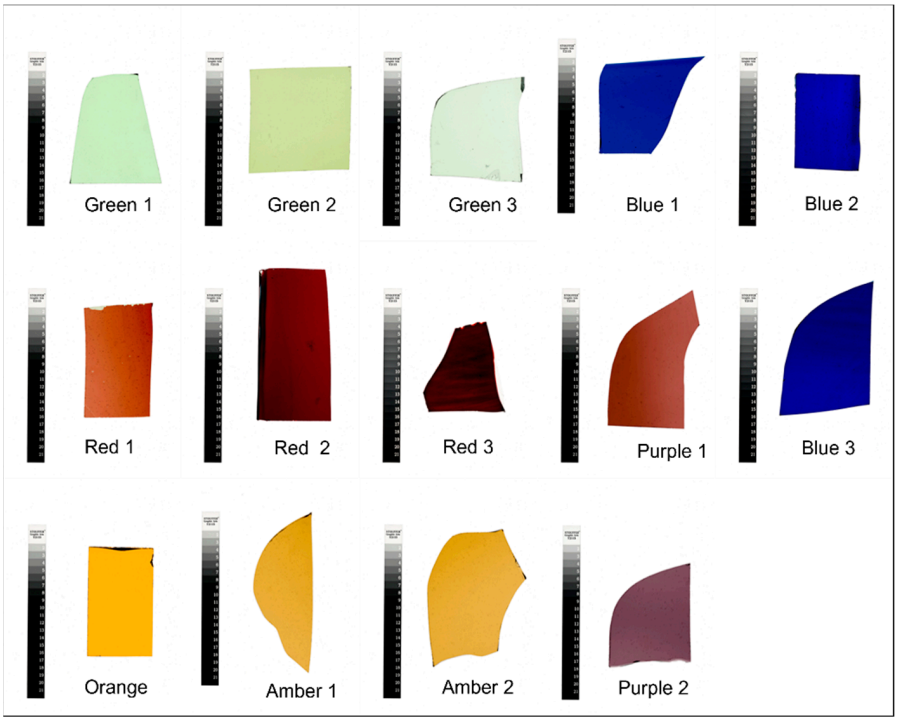

Figure 1. Glass samples photographed on a light table (credits to Ottar A.B. Anderson at SEDAK).

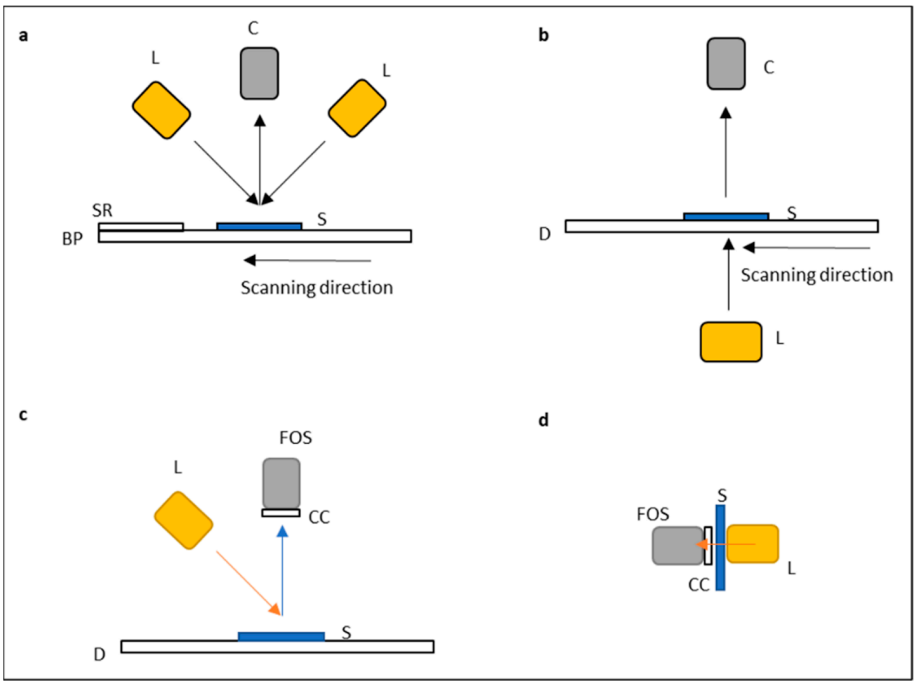

Figure 2. Schematic of the geometry for each instrument and measurement mode: (**a**) hyperspectral camera (reflectance), with the lights positioned at 45° (L) and the camera objective normal to the sample (S), which lays on the backing paper (BP). The standard reference (SR) is acquired together with the sample. In transmittance mode, (**b**) the light source is positioned below a diffuser panel (D), on top of which lies the glass sample in direct contact. The transmitted light is collected by the camera (C). (**c**) OceanOptics USB2000+ in reflectance mode and (**d**) in transmittance mode; the fiber-optic spectrometer (FOS) is equipped with a cosine corrector (CC) to diffuse the light.

Table 1. Instrument specifics.

	OceanOptics USB2000+	**HySpex VNIR-1800**
Type of instrument	Spectrometer	Hyperspectral camera
Type of measurement	Point analysis	Line scanning
Spectral range	180–890 nm	400–1000 nm
Spectral sampling	0.38–0.39 nm (2048 channels)	3.26 nm (186 bands)
Geometry	Reflectance:directional, 45:x:0 Transmittance: Diffuse efflux	Reflectance:directional, 45:a:0 Transmittance: Diffuse influx
Distance from sample	Around 0.5 cm	30 cm
Spot size	A few μm	Arbitrary selection of an area in the image
Light source	Tungsten-Halogen (Thorlabs)	Tungsten-Halogen

Two Spectralon references, one with 99% diffuse reflectance and one with 50% diffuse reflectance, were used to perform radiometric calibration for the OceanOptic USB2000+ and the hyperspectral camera, respectively.

The HySpex VNIR-1800 is a push-broom system, which means that the image is built line by line as the translation stage moves, while the camera and the light source stay fixed (Figure 2). This aspect is fundamental when performing the radiometric calibration; since the camera acquires one line at a time, it can be assumed that the signal collected and averaged from a few lines is representative of the light distribution across the whole field of view [32]. For this reason, only a small portion of the Spectralon reference was included in the image and used to calculate the reference spectrum. The radiometric-calibration step was carried out through the open-source software Fiji [33], following a procedure similar to that described in [28].

The reflectance was calculated as follows:

$$R_S = \frac{V_S}{V_{Ref}} * P_{Ref} \quad (1)$$

where R_S is the sample reflectance, V_S and V_{Ref} are the samples and the Spectralon radiance, respectively, and P_{Ref} is the certified-reflectance spectrum of the Spectralon reference, provided by the manufacturer. The dark current is automatically collected by the instrument in the beginning of the image acquisition.

In the case of HSI, radiometric calibration from radiance to transmittance was performed by simply dividing the radiance spectra of the sample by the radiance spectra of the diffusing panel (considered as reference), following the procedure described in [28]. With regards to the OceanOptic USB2000+, the reference was obtained by taking a measurement without the sample, collecting all the light coming from the light source, which was diffused by the cosine corrector. The radiometric calibration for the transmittance measurements was then calculated by dividing the spectra of each sample by the reference.

Since the calibration methods are different, some variation between the measured reflectance and transmittance spectra is expected, considering also that no calibration treatment was performed to improve the data. In all cases, the spectra were collected at the center of the glass pieces, where the glass was as homogeneous as possible.

2.2.2. Reflectance: Backing-Material Selection

For transmissive or translucent materials, the reflectance signal is strongly affected by light from the obverse. An alternative approach is to measure with only air as background, but in the proposed setup the sample is lain on a surface, and then the reflectance of this surface through the glass inevitably affects the signal. To overcome this issue, a non-spectrally selective backing substrate (perfect white diffuser) can be used to calibrate the reflectance. In the field of cultural heritage, a similar approach has been used in the work of Rebollo et al. [24] to analyze the stained glass windows of the Scrovegni Chapel (Padua, Italy). The influence of backing material on the result of reflectance measurements is

an important aspect that must be considered when working with transparent materials. According to the ISO 13655:2017 standard recommendations [31], the backing material should be free of optical brighteners, in order to avoid unwanted artifacts in the spectra, especially in the UV region. The backing material for reflectance measurements was, thus, carefully selected to be as compliant as possible with the recommendation proposed in the ISO 13655:2017 standard. Two paper sheets were compared for the purpose: the first one is a commercially available inkjet paper, while the second one is a IGT Reference paper C2846 [34].

The two sheets were analyzed with the OceanOptic USB2000+ spectrometer before the beginning of the experiment. Note that in this case the intensity range is between 0–100 because the data were collected directly in reflectance using the spectrometer software. For the rest of the experiment, on the other hand, the reflectance was calculated manually from radiance data. The measurements were repeated placing one of the green-glass pieces (Green 1) over each sheet. Green 1 was selected for this part of the experiment due to its specific peak in the UV region, which is the most influenced by the effects of composition and treatment of the paper. It can be noticed that the reflectance of the inkjet paper sheet (Figure 3, gray dotted line) drops at around 350 nm which may be related to the presence of optical brightener, consequently leading to artifacts in the reflectance spectrum of the green glass.

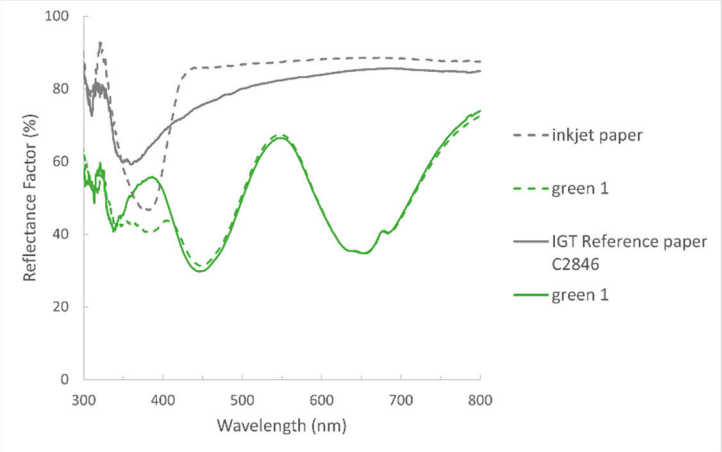

Figure 3. Effects of the backing material are clearly visible in the spectral shape of the sample Green 1, especially in the UV region. The peak at around 380 nm is visibly distorted when the first type of paper is used as background.

2.2.3. Complementary Analysis

XRF analysis was performed by means of a Thermo Scientific Niton XL3t handheld XRF spectrometer, equipped with a silver anode and a GOLDD detector. The acquisition time was set at 120 s and the voltage at 40 kV for each measurement. Note that the instrument is not equipped with a program for glass analysis, and the measurements were performed in Cu/Zn mining mode. Moreover, the measurements could not be calibrated against glass standards as they were unavailable. For this reason, the results obtained must be considered only from a qualitative point of view. The Niton NDT software was used for the spectra interpretation. Three points were collected across the surface of each glass piece, to verify the homogeneity of the glass. The exact positions of the points are shown in Figure S15, available in the Supplemental Material.

2.3. FORS and HSI Performance Evaluation

To evaluate the performance of the two instruments, the CIELAB L*a*b* values and the color difference ΔE were calculated as suggested in ISO/TS 23031 for the inter-model agreement [35]. To calculate the L*a*b* values, the spectral data were first converted to XYZ, using the CIE 1931-2° Standard Observer Color Matching Function and CIE standard

illuminant D65 [36]. L*a*b* values were obtained using the formula in CIE 15:2004 [30], using the D65 reference white values for X, Y, and Z. The formula was implemented in MATLAB through the Color Engineering Toolbox [37].

The color difference ΔE_{00} was calculated using the CIEDE2000 formula [30,38,39] through the same toolbox [37], setting the USB2000+ as reference, both for transmittance and for reflectance. The reproducibility of the measurements was not evaluated.

It is worth mentioning that there is no ground truth for these glass samples; their optical properties and composition have not been measured quantitatively yet, and the interpretation of the spectra could be only made by comparing the results with the existing literature and qualitative pXRF analysis. For these reasons, the color differences have only been reported, and no statistical treatment has been performed on them.

3. Results

The result section is divided into two parts. In the first part, the chromophores responsible for the color of each glass piece are discussed, to show how these elements influence the color of the samples. Results from qualitative XRF analysis are used as supporting information; the chromophore elements identified are summarized in Table 2 for each glass piece, listed in reverse order of their contribution to the color formation. XRF spectra of each sample are provided as Supplementary Material (S1–S14). Some results for the darkest samples were omitted (two of the blue glass) because they were considered too noisy and not significant. The results of the two amber samples were included in the same plot, since they have the same composition.

Table 2. List of elements contributing to the color of the glass samples ordered from the most to the least abundant.

	Chromophores
Green 1	Cr, Cu, Fe
Green 2	Fe, Cr, Mn (decoloring), Cu
Green 3	Mn (decoloring), Fe
Blue 1	Cu, Fe, Co, Mn (decoloring)
Blue 2	Fe, Mn (decoloring?), Cu, Co
Blue 3	Cu, Fe, Mn (decoloring?), Co
Red 1	Red layer: Cu. Uncolored layer: Fe, Mn (decoloring)
Red 2	Red layer: Cu, Sn, Sb. Uncolored layer (?): Fe, Mn (decoloring)
Red 3	Red layer: Cu, Sn, Sb. Uncolored layer (?): Fe, Mn (decoloring)
Orange	Fe
Amber 1 and 2	Mn (decoloring), Fe
Purple 1	Mn (colorant), Fe
Purple 2	Mn (colorant), Fe, Co

In the second part, the glasses L*a*b values from each instrument and modality, together with the color difference ΔE_{00}, are reported.

3.1. Chromophore Identification

3.1.1. Green Glass

All the spectra of the green samples show a good agreement and are very easy to identify. The reason behind this good agreement may be that, compared to the other samples, the green glasses are relatively thin and present a very flat surface with almost no defects. The presence of bubbles inside the glass does not seem to create interference as it was possible to find areas without them for measurements.

Sample Green 1 and Green 2 (Figure 4a,b) show a similar spectrum, with an absorption band centered at 450 nm and two bands at around 658 and 686 nm, which are characteristic of chromium (Cr^{3+}) [17,20,22,24,40]. A third band is barely visible at around 638 nm, especially in the reflectance modality.

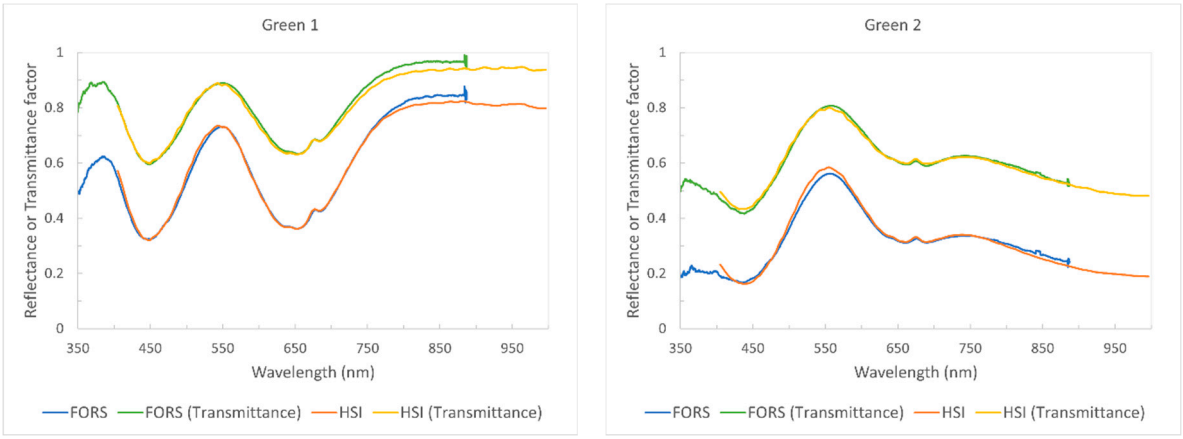

(**a**) (**b**)

Figure 4. (**a**) Spectra comparison for sample Green 1; (**b**) spectra comparison for sample Green 2.

Sample Green 2 appears to contain a higher amount of iron, suggested by the more pronounced absorption band at the end of the NIR region [22], which is confirmed by XRF analysis. The band in the NIR region usually has a maximum at around 1100 nm (out of the range of the instruments) and is associated with iron as Fe^{2+}, which gives a yellow color to glass [12,16,18,22,41,42]; this explains the more yellowish appearance of the sample Green 2, and, consequently, the highest values of b* among the three green samples.

The spectra of the Green 3 (Figure 5) sample on the other end are very different from the others. In this case, the color is given only by iron.

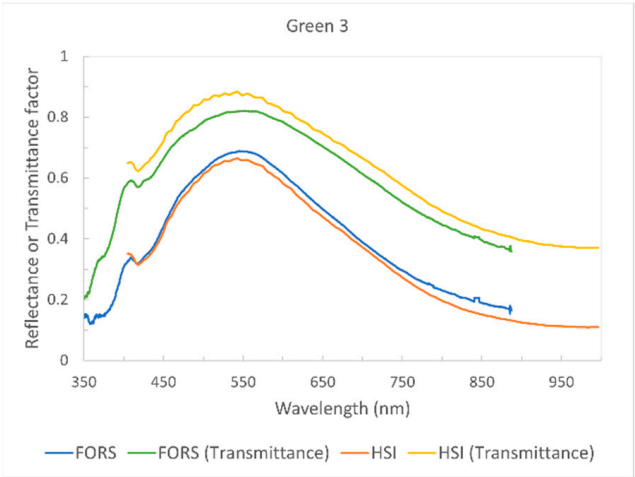

Figure 5. Spectra comparison for sample Green 3.

Here, iron is present both as Fe^{2+} and Fe^{3+}, as suggested by the three small absorption bands at 380, 420, and 435–440 nm, associated with Fe^{3+}, and the broad band of Fe^{2+} in the NIR region [12,16,18,22,41,42]. Fe^{3+} gives a blue color to glass. Thus, the pale-green color of the glass is due to the redox equilibrium between Fe^{3+} and Fe^{2+} species. Manganese, in its oxidation state Mn^{2+}, also has an absorption band at 420 nm, which in some papers is referred to as the Fe/Mn complex band [11,12,16,18,22,41,42]. Since Mn^{2+} is uncolored, it could have been used as a decoloring agent.

3.1.2. Blue Glass

The three blue-glass pieces are characterized by a very dark color, and, consequently, the magnitudes of the spectra obtained are very low, especially in the case of samples Blue 2 and 3. These two glass pieces are among the thickest samples in the group and also have

a very rough surface. In reflectance mode, it is difficult to distinguish the signature peaks of the coloring agents used; in this case, transmittance measurements are more helpful as the characteristic bands become more visible. Note that the FORS' reflectance results for sample Blue 2 and HSI's reflectance results for samples Blue 2 and 3 were discarded, as they did not provide satisfying results. For this reason, the color difference was calculated only for the Blue 1 sample, as it was the only one that gave sufficiently good spectra for all the instruments.

The shape of the spectra suggests that the three samples were colored using a distinct combination of chromophores. This is confirmed by the XRF analysis, which identified cobalt, copper, and iron in different concentrations. The three signature bands of cobalt (Co^{2+}) at around 530–540, 590–600, and 650–670 nm can be observed in Blue 1, while in Blue 2 and 3, the last two bands are barely visible [3,12,16,20,24,40,43] (Figure 6).

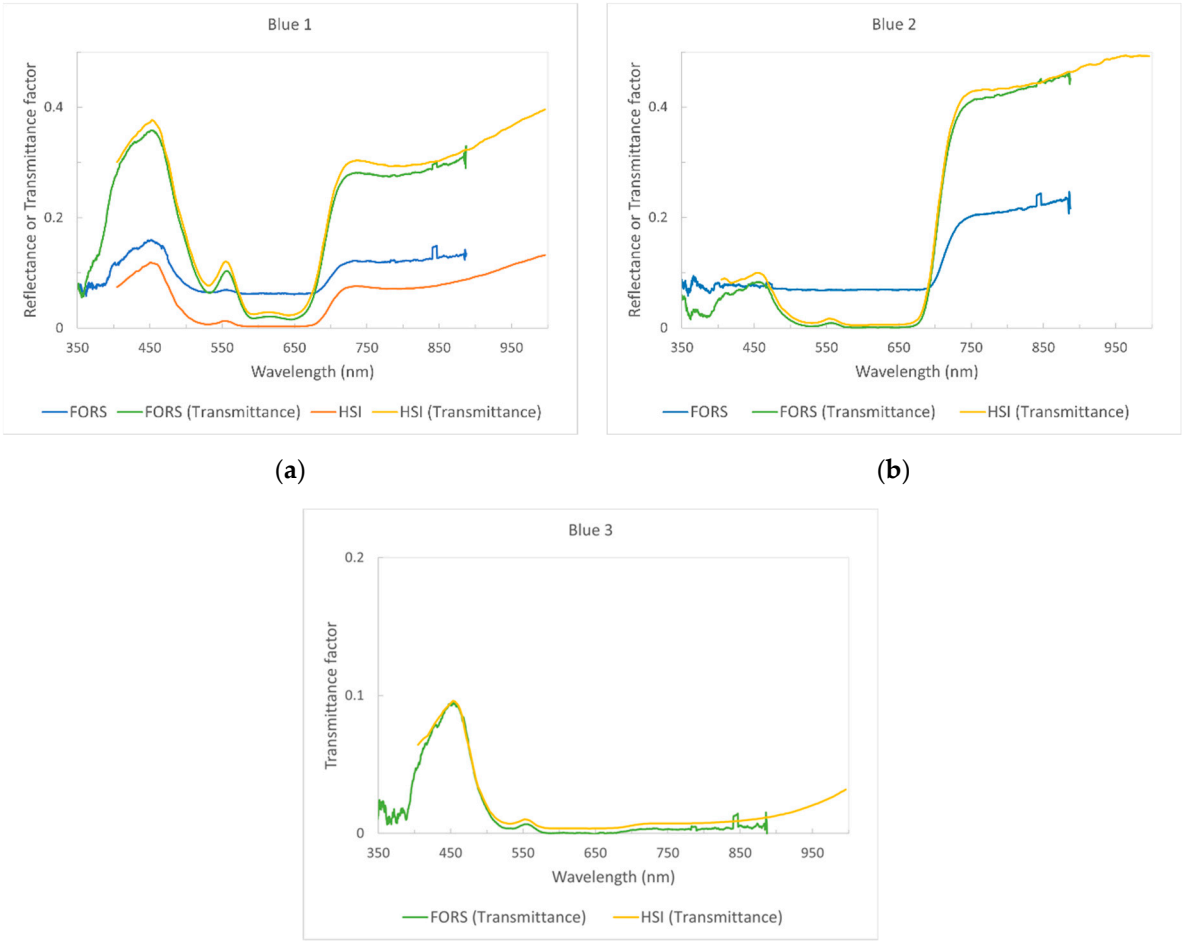

Figure 6. (**a**) Spectra comparison for sample Blue 1; (**b**) spectra comparison for sample Blue 2; (**c**) spectra comparison for sample Blue 3.

The absorption band centered at around 780–790 nm in samples Blue 1 and 3 suggests that copper could have been used as an additional coloring agent as Cu^{2+} [3,15,16,20] and probably in higher concentrations in sample Blue 1, as confirmed by XRF analysis.

3.1.3. Red Glass

The production of red glass is very different from the other type of colored glass. Obtaining a red glass in the past was challenging, as even a small amount of colorant in the glass body was enough to produce a deeply colored glass, too dark to be employed in a

window [2]. To overcome this problem, the red color was achieved by adding a thin red layer made of copper nanoparticles over a transparent one. This could have been made in two ways, by alternating multiple thin red layers and transparent ones (feuilletes) or by applying a single red layer over a thicker colorless glass (plaques) [44–46]. The glass pieces studied in this paper belong to the second category. The red layers of these samples are characterized by different hues and thickness, going from a thin, pale red layer (Red 1) to a thicker and darker one (Red 3).

Sample Red 1 (Figure 7a) is the only one among the three red glass that clearly shows the characteristic absorbance bands related to the surface plasmonic resonance (SPR) of the copper nanoparticles (at around 565 nm) [3–6,10,19,20,24,45] and the one at 430 nm, which could be related to isolated Cu^0 atoms [3,5,24]. This is especially visible in transmittance mode. In Red 2 (Figure 7b), only the band at 565 nm is visible, while the one at 430 nm is completely absent. The reason behind this is not clear yet; the available literature suggests that it could be related to variation in the roughness of the red layer [4], the size of the copper particles, the annealing temperature during the formation of the colored layer, or its chemical composition [14,47].

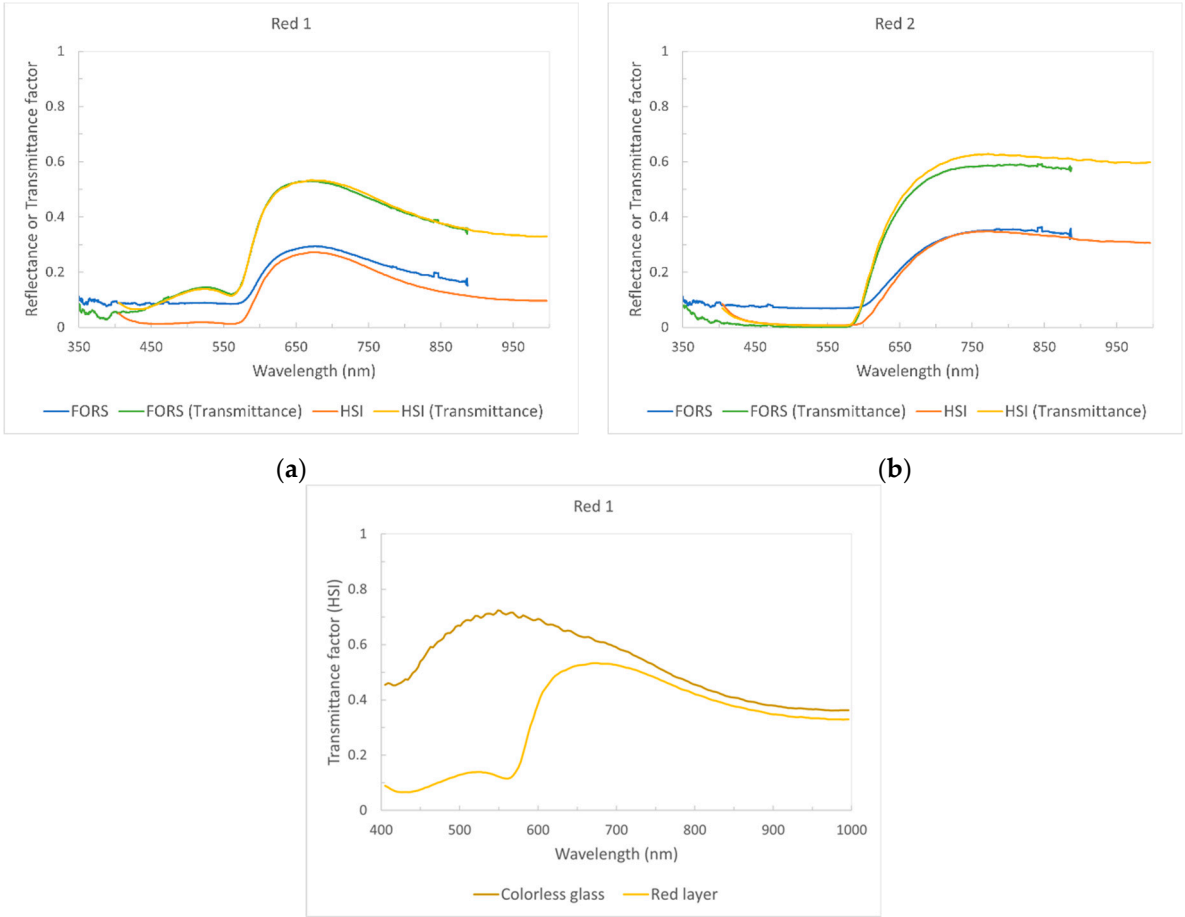

Figure 7. (**a**) Spectra comparison for sample Red 1; (**b**) spectra comparison for sample Red 2; (**c**) spectra comparison between the two layers of Red 1.

In addition to copper, the presence of Fe^{2+} in both samples can be inferred by the presence of its absorption band at 1000 nm, which is more intense in sample Red 1 [10,19,20], even if XRF analysis detected a higher amount of iron in sample Red 2. Most probably, Fe^{2+} does not contribute to the red color of the thin layer but could be present in the colorless layer (which appears slightly yellowish) as an intentional addition or impurity. In the case

of Red 1, this conjecture seems to be confirmed by comparing spectra taken from the red layer and the transparent layer (Figure 7c). Unfortunately, a similar comparison could not be made with sample Red 2, as there are no areas where the transparent layer is accessible.

The Red 3 sample (Figure 8) is quite different from the other two glass pieces: it shows a more significant difference between the reflectance and the transmittance spectra, not only in intensity but also in shape.

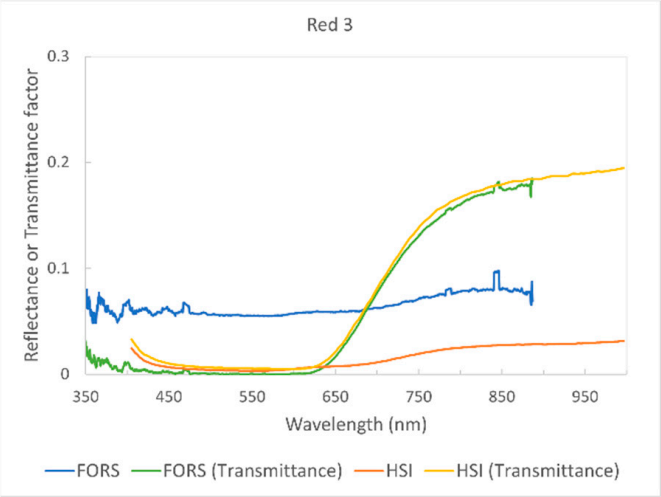

Figure 8. Spectra comparison for sample Red 3.

In reflectance modality, for example, an additional band appears at around 680–700 nm, while in transmittance, the absorption band of the copper nanoparticles is shifted toward longer wavelengths, at about 630 nm.

Red 3 has very low and sometimes negative values of CIELAB b*, hinting at a more bluish hue compared to the other two red-glass pieces. Bring and Jonson [14] suggest that the presence of antimony (as Sb^{3+}) and tin (as Sn^{2+}) can play an important role in the coloring process of the red layer. A significant amount of antimony and tin has been found in Red 2 and 3 by XRF, with Red 3 having a lower quantity of antimony than Red 2; according to Bring and Jonson a smaller concentration of Sb^{3+} can give a deep red color with a bluish tint to the glass [14]. This observation seems to be consistent with the combined results from the FORS, HSI, and XRF for Red 3. Nonetheless, additional quantitative or semi-quantitative analyses are necessary to confirm this hypothesis.

It is also interesting to notice how the L* value from the fiber spectrometer in transmittance is extremely low (see Colorimetry subsection). This is probably caused by the great thickness and dark color of the red layer, which may have prevented the light from being transmitted through the sample, generating a very low signal. On the other hand, the L* values obtained in reflectance are relatively high, indicating that the first surface reflectance of sample Red 3 has a higher contribution. However, the data obtained with the HSI show an opposite trend, with the two values of L* (reflectance and transmittance) being almost comparable. This likely arises from the different optical designs of the instruments.

3.1.4. Orange and Amber Glass

The spectra of both orange and amber samples show differences in intensity and shape when comparing the results obtained in the two modalities (Figure 9).

For the three glass pieces, more than in other samples, the absorption bands of the spectra collected in transmittance shift to shorter wavelengths with respect to those acquired in reflectance, hinting at a more yellowish color. This phenomenon is also confirmed by visual inspection and from the CIELAB L* a*b* values (see Colorimetry subsection); in both cases, the a* values calculated in transmittance are lower than that in reflectance, while the b* values remain quite similar.

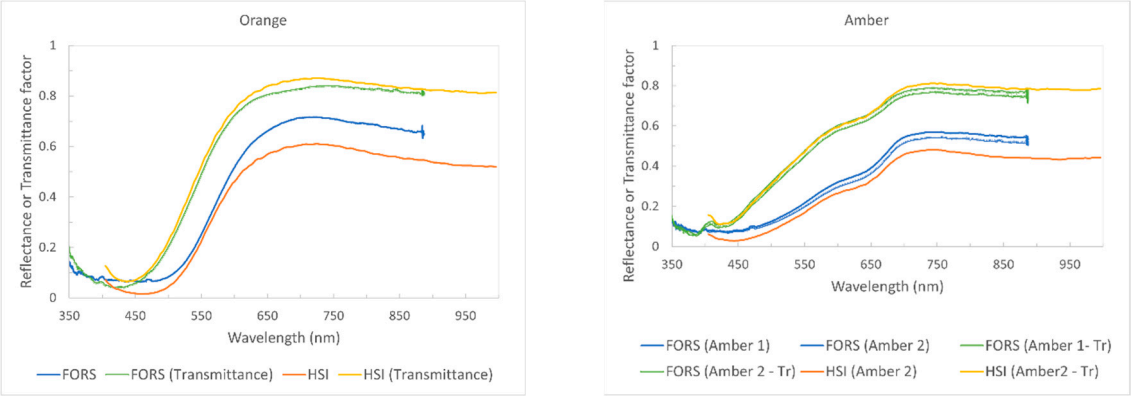

(**a**) (**b**)

Figure 9. (**a**) Spectra comparison for sample Orange; (**b**) spectra comparison for sample Amber.

Since the two amber pieces come from the same batch and, thus, have the same composition, their results were grouped in the same plot. The results obtained with the FORS show a difference in magnitude between the two samples, both in transmittance and in reflectance. Interestingly, in transmittance mode, the spectra taken from Amber 1 with the fiber optic agrees more with the spectra taken from Amber 2 with the HSI, as opposed to the Amber 2 spectra taken with the fiber at almost the same location. This could mean that, in this case, the characteristic of the surface greatly influences the result, and particular care must be taken when selecting the areas from which to collect the spectra.

From the chemical point of view, according to the available literature, the orange/amber color in the glass is given by the ferric iron-sulfide (Fe^{3+}-S) complex. This chromophore can be recognized by a broad absorption band at around 410 nm [4,10,12,13,16,20,42,48]. The shallow, broad band at around 1000 nm suggests that iron could be present also as Fe^{2+}. Iron was detected by XRF analysis in both samples, confirming the involvement of this element in the glass coloration; sulfur was found as well, but the amount is too small, especially compared to other glass, to make any solid conclusion on the presence of the iron-sulfide (Fe^{3+}-S) complex. Further analyses are necessary to have a clear understanding of the coloring process of this glass, as well as the reason behind the color shifting between transmittance and reflectance.

Compared to the orange sample, the amber fragments also seem to contain a consistent amount of manganese, probably as uncolored Mn^{2+} [13]; the presence of this oxide could be suggested by a small band at 420 nm, which is visible only in the spectra obtained by the FORS in transmittance mode [16]. Despite some shifting in the position of the absorbance band, the shape of the spectra obtained for the orange pieces in this experiment is consistent with the results found in previous works. Regarding the amber glass, however, the extra band at around 630–650 nm is difficult to interpret; no other example exists in the available literature, except for the work of Bacon and Billian [48], which unfortunately does not explain the nature of this band.

3.1.5. Purple Glass

The two glass pieces clearly show a difference in composition, which also explains the difference in color (Figure 10).

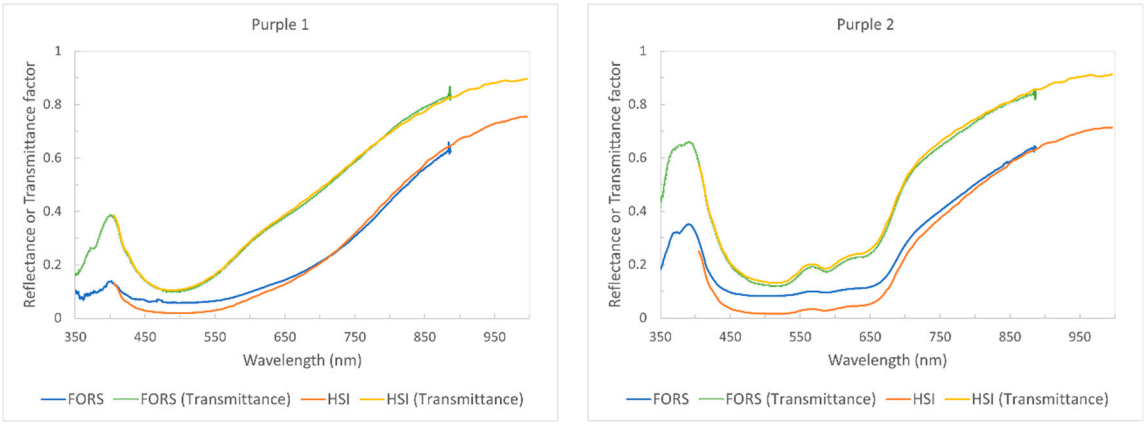

(**a**) (**b**)

Figure 10. (**a**) Spectra comparison for sample Purple 1; (**b**) spectra comparison for Purple 2.

The first sample (Purple 1) has a warm-purple, almost brownish color, while the second one (Purple 2) appears more bluish. This observation is confirmed by the calculated values of b*, which are positive for the first sample and negative for the other (see Colorimetry subsection). From a chemical point of view, the different color is due to the fact that for sample Purple 1 the main chromophore is manganese (Mn^{3+}), characterized by a broad band at around 500–490 nm and a shoulder at about 670 nm, with a small contribution of iron (as Fe^{3+}) [4,9,11,16,20,22,24,42,49], while in Purple 2 the three absorption bands at around 525, 590, and 650 nm suggest that cobalt (Co^{2+}) has been added to give a more bluish hue [4,50].

3.2. Colorimetry

3.2.1. CIELAB L*a*b* Values

Tables 3–14 report the CIELAB L*a*b* values of each colored glass, calculated from the spectra obtained with FORS and HSI in transmittance and reflectance mode.

Table 3. L*a*b* values for sample Green 1.

Green 1	L*	a*	b*
USB2000+ (Tr)	92.26	−13.63	13.83
HySpex VNIR-1800 (Tr)	92.04	−14.50	13.83
USB2000+	82.33	−24.98	25.03
HySpex VNIR-1800	82.54	−26.21	25.24

Table 4. L*a*b* values for sample Green 2.

Green 2	L*	a*	b*
USB2000+ (Tr)	88.76	−13.36	24.44
HySpex VNIR-1800 (Tr)	88.54	−13.51	23.22
USB2000+	74.36	−19.89	35.95
HySpex VNIR-1800	75.49	−22.13	38.62

Table 5. L*a*b* values for sample Green 3.

Green 3	L*	a*	b*
USB2000+ (Tr)	91.51	−7.53	9.70
HySpex VNIR-1800 (Tr)	93.87	−8.44	8.91
USB2000+	84.19	−14.25	17.64
HySpex VNIR-1800	82.83	−14.87	17.28

Table 6. L*a*b* values for sample Blue 1.

Blue 1	L*	a*	b*
USB2000+ (Tr)	33.43	15.35	−50.88
HySpex VNIR-1800 (Tr)	35.87	12.68	−48.66
USB2000+	31.62	9.64	−45.49
HySpex VNIR-1800	10.47	29.18	−21.52

Table 7. L*a*b* values for sample Red 1.

Red 1	L*	a*	b*
USB2000+ (Tr)	52.65	29.77	30.28
HySpex VNIR-1800 (Tr)	52.13	30.76	29.59
USB2000+	40.70	22.13	9.30
HySpex VNIR-1800	28.04	41.83	26.11

Table 8. L*a*b* values for sample Red 2.

Red 2	L*	a*	b*
USB2000+ (Tr)	25.62	58.38	33.33
HySpex VNIR-1800 (Tr)	27.96	56.97	22.65
USB2000+	33.87	13.25	1.137
HySpex VNIR-1800	16.25	37.07	0.90

Table 9. L*a*b* values for sample Red 3.

Red 3	L*	a*	b*
USB2000+ (Tr)	0.99	6.15	−1.30
HySpex VNIR-1800 (Tr)	5.71	7.90	−6.54
USB2000+	28.44	1.37	−1.45
HySpex VNIR-1800	3.74	5.12	−4.45

Table 10. L*a*b* values for the Amber samples.

Amber	L*	a*	b*
USB2000+ (Tr)			
Amber 1	75.00	3.92	43.77
Amber 2	73.47	4.41	44.70
HySpex VNIR-1800 (Tr)	74.75	3.88	44.92
USB2000+			
Amber 1	55.41	11.91	33.89
Amber 2	53.51	12.19	32.27
HySpex VNIR-1800	49.98	12.18	44.92

Table 11. L*a*b* values for sample Orange.

Orange	L*	a*	b*
USB2000+ (Tr)	76.31	13.31	72.35
HySpex VNIR-1800 (Tr)	78.05	12.26	69.34
USB2000+	62.20	28.91	52.36
HySpex VNIR-1800	58.65	27.20	70.37

Table 12. L*a*b* values for sample Purple 1.

Purple 1	L*	a*	b*
USB2000+ (Tr)	50.68	24.66	9.01
HySpex VNIR-1800 (Tr)	51.42	23.94	9.59
USB2000+	33.13	13.40	2.84
HySpex VNIR-1800	24.78	23.29	6.88

Table 13. L*a*b* values for sample Purple 2.

Purple 2	L*	a*	b*
USB2000+ (Tr)	47.80	18.35	−9.21
HySpex VNIR-1800 (Tr)	49.37	17.02	−7.65
USB2000+	33.74	8.83	−6.24
HySpex VNIR-1800	19.25	17.89	−9.64

Table 14. Summary table of color differences ΔE_{00}.

ΔE_{00}	USB2000+ (Tr) vs. HySpex1800 (Tr)	USB2000+ vs. HySpex1800	USB2000+ (Tr) vs. USB2000+	HySpex1800 (Tr) vs. HySpex1800
Green 1	0.73	0.59	9.70	9.62
Green 2	0.69	1.48	**11.10**	**11.14**
Green 3	1.85	1.05	7.89	9.43
Red 1	0.97	**14.58**	**16.47**	**22.25**
Red 2	5.43	**17.52**	**21.75**	**14.51**
Red 3	4.71	**17.19**	**18.90**	3.31
Blue 1	3.01	**19.99**	9.04	**22.55**
Orange	1.47	7.53	**17.71**	**17.61**
Amber				**21.90**
Amber 1	0.43	6.85	**17.92**	
Amber 2	1.03	6.22	**18.82**	
Purple 1	0.96	9.12	**17.56**	**22.89**
Purple 2	1.96	**12.80**	**14.42**	**24.59**
Average	**1.94**	**9.58**	**15.09**	**16.34**

3.2.2. Color Difference ΔE_{00}

The color difference values calculated between the FORS and HSI transmittance and reflectance measurements and between transmittance and reflectance measurements from the same instrument are reported in Table 14. Values above 10 are shown in bold. For the comparison of transmittance between the FORS and HSI, values that are clearly higher than those of most colored pieces are underlined.

4. Discussion

From the point of view of the spectra, the results obtained with HSI are consistent with those produced by the FORS, especially in transmittance mode. Regarding reflectance, a difference in intensity between the FORS and HSI spectra can be noticed in many samples; in general, the spectra obtained by the FORS have a higher intensity than the hyperspectral ones, especially in the case of the darkest samples (Red 2, Red 3, Blue 1). The trend described above is also demonstrated by the ΔE_{00} values calculated between the FORS and HSI in reflectance mode, which are almost always very high. During the experiments, it was observed that the fiber optic seems quite sensitive to the distance from the sample, as also noted in [45], and this fact may have influenced the results. The different geometries and radiance correction procedures of the two instruments could also be other factors that affected the measurements. The fiber optic may be more sensitive to the stray light reflected from the surface of the darkest samples, generating errors during the preprocessing phase.

On the other hand, the FORS and the HSI can generate comparable results when used in transmittance mode. The ΔE_{00} values calculated between the FORS and HSI are relatively low in almost every case, with the darkest samples showing the relatively highest color difference, as shown in Table 14.

The shape of the spectra remains almost always unchanged, regardless of the instrument or modality, except for amber and darker red and blue samples (Red 2, Red 3, Blue 1, Blue 2). Comparing the transmittance and reflectance spectra of amber glass, for example, the absorption bands show a considerable variation in width, which may be related to how the light is reflected, transmitted, and scattered by the glass sample and how the sensor of the instrument collects this light. Regarding the darker glass, the reflectance modality does not perform very well, as most of the light gets absorbed while traveling twice through the glass, so a poor performance can be expected. From a colorimetric point of view, this behavior is shown by higher differences in L* values between reflectance and transmittance modality for dark-colored glass. In contrast, this difference is less pronounced in the lighter glass. From the spectral point of view, the characteristic peaks of strongly colored glass are entirely lost in reflectance mode, especially in the case of the blue- and red-glass pieces, while visible in transmittance mode. On the other hand, the reflectance modality is very helpful in enhancing the intensity of small peaks in light-colored glass, as previously noted in the work of Rebollo et al. [26]. This can be noticed, for example, in all the green glass, where the weak peaks of iron (Fe^{3+}) and chromium (Cr^{3+}) can be better appreciated in reflectance modality.

5. Conclusions

In this paper, we compared the performance of a fiber-optic spectrometer and a hyperspectral camera in measuring colored glass. The results demonstrated that the two instruments could produce comparable results, especially in transmittance modality. On the other hand, reflectance measurements generated mixed results; in general, there is an apparent disagreement between the reflectance results obtained by the two instruments, especially for very dark glass.

Regardless of the measuring geometries, an advantage of using both instruments lies in the spectral range. In fact, the two devices complement each other, as the FORS and the hyperspectral camera have an extended range in the UV and the IR region. respectively, which allows a more complete characterization of the chromophores used in the colored glass.

Considering future works, a better understanding of the complex interaction between the glass and light would be necessary to explain the differences in the spectral shape, when measuring in different geometries. In this sense, it would be interesting to perform spectral acquisitions from other angles, to understand how much the spectral shape and intensity, and consequently the color, can change within the same sample. In addition, further analysis should be performed to better characterize the chromophores involved in the coloration of the glass pieces.

Future works should also be focused on adjusting the calibration procedure to improve the agreement between the instruments, both in transmittance mode and in reflectance mode.

Supplementary Materials: The following supporting information can be downloaded at: https://www.mdpi.com/article/10.3390/heritage5030073/s1, Figures S1–S14: pXRF data of each glass; Figure S15: location of points analyzed with XRF.

Author Contributions: Conceptualization, A.B., P.G., S.G. and J.Y.H.; methodology, A.B. and P.G.; validation, A.B. and P.G.; formal analysis, A.B.; investigation, A.B.; data curation, A.B.; writing—original draft preparation, A.B.; writing—review and editing, A.B., P.G., S.G. and J.Y.H.; visualization, A.B.; supervision, P.G., S.G. and J.Y.H.; project administration, S.G.; funding acquisition, J.Y.H. All authors have read and agreed to the published version of the manuscript.

Funding: This project has received funding from the European Union's Horizon 2020 research and innovation programme under the Marie Skłodowska–Curie grant no. 813789 (CHANGE-ITN).

Institutional Review Board Statement: Not applicable.

Informed Consent Statement: Not applicable.

Data Availability Statement: Data are available upon request. Please contact the corresponding author.

Acknowledgments: The authors would like to thank Elizabeth Sinnerud at the Nidaros Cathedral Restoration Workshop (Trondheim) for providing the glass pieces used for the experiments; Jan Cutajar at the University of Oslo (UiO) for carrying out the XRF measurements; and Ottar A.B. Anderson at SEDAK for the high-quality pictures of the samples.

Conflicts of Interest: The authors declare no conflict of interest.

References

1. Babini, A.; George, S.; Lombardo, T.; Hardeberg, J.Y. Potential and Challenges of Spectral Imaging for Documentation and Analysis of Stained-Glass Windows. *Lond. Imaging Meet.* **2020**, *2020*, 109–113. [CrossRef]
2. Fornacelli, C.; Colomban, P.; Memmi, I.T. Toward a Raman/FORS discrimination between Art Nouveau and contemporary stained glasses from CdSxSe1-x nanoparticles signatures. *J. Raman Spectrosc.* **2015**, *46*, 1129–1139. [CrossRef]
3. Bacci, M.; Corallini, A.; Orlando, A.; Picollo, M.; Radicati, B. The ancient stained windows by Nicolo di Pietro Gerini in Florence. A novel diagnostic tool for non-invasive in situ diagnosis. *J. Cult. Herit.* **2007**, *8*, 235–241. [CrossRef]
4. Bracci, S.; Bartolozzi, G.; Burnam, R.K.; Corallini, A. Integration of both non-invasive and micro-invasive techniques for the archaeometric study of the stained-glass window Apparizione degli Angeli in the basilica of Santa Croce in Florence, Italy. *J. Cult. Herit.* **2020**, *44*, 307–316. [CrossRef]
5. Meulebroeck, W.; Wouters, H.; Nys, K.; Thienpont, H. Authenticity screening of stained glass windows using optical spectroscopy. *Sci. Rep.* **2016**, *6*, 37726. [CrossRef] [PubMed]
6. Palomar, T.; Agua, F.; Garcia-Heras, M.; Villegas, M.A. Chemical degradation and chromophores of 18(th) century window glasses. *Glass Technol.-Eur. J. Glass Sci. Technol. Part A* **2011**, *52*, 145–153.
7. Meulebroeck, W.; Baert, K.; Ceglia, A.; Cosyns, P.; Wouters, H.; Nys, K.; Terryn, H.; Thienpont, H. The potential of UV-VIS-NIR absorption spectroscopy in glass studies. In Proceedings of the Integrated Approaches to the Study of Historical Glass—Ias12, Brussels, Belgium, 16–17 April 2012; Volume 8422.
8. Kaplan, Z.; İpekoğlu, B.; Böke, H. Physicochemical properties of glass tesserae in Roman terrace house from ancient Antandros (base glass, opacifiers and colorants). *Mediterr. Archaeol. Archaeom.* **2017**, *17*, 141–157.
9. Rodrigues, A.; Coutinho, M.; Machado, A.; Martinho, B.A.; Cerqueira Alves, L.; Macedo, M.F.; Vilarigues, M. A transparent dialogue between iconography and chemical characterisation: A set of foreign stained glasses in Portugal. *Herit. Sci.* **2021**, *9*, 22. [CrossRef]
10. Hunault, M.O.J.Y.; Bauchau, F.; Boulanger, K.; Hérold, M.; Calas, G.; Lemasson, Q.; Pichon, L.; Pacheco, C.; Loisel, C. Thirteenth-century stained glass windows of the Sainte-Chapelle in Paris: An insight into medieval glazing work practices. *J. Archaeol. Sci. Rep.* **2021**, *35*, 102753. [CrossRef]
11. Bidegaray, A.-I.; Godet, S.; Bogaerts, M.; Cosyns, P.; Nys, K.; Terryn, H.; Ceglia, A. To be purple or not to be purple? How different production parameters influence colour and redox in manganese containing glass. *J. Archaeol. Sci. Rep.* **2019**, *27*, 101975. [CrossRef]
12. Micheletti, F.; Orsilli, J.; Melada, J.; Gargano, M.; Ludwig, N.; Bonizzoni, L. The role of IRT in the archaeometric study of ancient glass through XRF and FORS. *Microchem. J.* **2020**, *153*, 104388. [CrossRef]
13. Schreurs, J.W.H.; Brill, R.H. Iron and Sulfur Related Colors in Ancient Glasses. *Archaeometry* **1984**, *26*, 199–209. [CrossRef]
14. Bring, T.; Jonson, B.; Kloo, L.; Rosdahl, J. Colour development in copper ruby alkali silicate glasses: Part 2. The effect of tin (II) oxide and antimony (III) oxide. *Glass Technol.-Eur. J. Glass Sci. Technol. Part A* **2007**, *48*, 142–148.
15. Hunault, M.; Bauchau, F.; Loisel, C.; Herold, M.; Galoisy, L.; Newville, M.; Calas, G. Spectroscopic Investigation of the Coloration and Fabrication Conditions of Medieval Blue Glasses. *J. Am. Ceram. Soc.* **2016**, *99*, 89–97. [CrossRef]
16. Möncke, D.; Papageorgiou, M.; Winterstein-Beckmann, A.; Zacharias, N. Roman glasses coloured by dissolved transition metal ions: Redox-reactions, optical spectroscopy and ligand field theory. *J. Archaeol. Sci.* **2014**, *46*, 23–36. [CrossRef]
17. Hunault, M.; Lelong, G.; Gauthier, M.; Gelebart, F.; Ismael, S.; Galoisy, L.; Bauchau, F.; Loisel, C.; Calas, G. Assessment of Transition Element Speciation in Glasses Using a Portable Transmission Ultraviolet-Visible-Near-Infrared (UV-Vis-NIR) Spectrometer. *Appl. Spectrosc.* **2016**, *70*, 778–784. [CrossRef]
18. Meulebroeck, W.; Wouters, H.; Baert, K.; Ceglia, A.; Terryn, H.; Nys, K.; Thienpont, H. *Optical Spectroscopy Applied to the Analysis of Medieval and Post-Medieval Plain Flat Glass Fragments Excavated in Belgium*; SPIE: Bellingham, WA, USA, 2010; Volume 7726.
19. Hunault, M.O.J.Y.; Loisel, C.; Bauchau, F.; Lemasson, Q.; Pacheco, C.; Pichon, L.; Moignard, B.; Boulanger, K.; Herold, M.; Calas, G.; et al. Nondestructive Redox Quantification Reveals Glassmaking of Rare French Gothic Stained Glasses. *Anal. Chem.* **2017**, *89*, 6278–6649. [CrossRef]

20. Capobianco, N.; Hunault, M.O.J.Y.; Balcon-Berry, S.; Galoisy, L.; Sandron, D.; Calas, G. The Grande Rose of the Reims Cathedral: An eight-century perspective on the colour management of medieval stained glass. *Sci. Rep.* **2019**, *9*, 3287. [CrossRef]
21. Molina, G.; Murcia, S.; Molera, J.; Roldan, C.; Crespo, D.; Pradell, T. Color and dichroism of silver-stained glasses. *J. Nanopart. Res.* **2013**, *15*, 1932. [CrossRef]
22. Meulebroeck, W.; Baert, K.; Wouters, H.; Cosyns, P.; Ceglia, A.; Cagno, S.; Janssens, K.; Nys, K.; Terryn, H.; Thienpont, H. *The Identification of Chromophores in Ancient Glass by the Use of UV-VIS-NIR Spectroscopy*; SPIE: Bellingham, WA, USA, 2010; Volume 7726.
23. Meulebroeck, W.; Cosyns, P.; Baert, K.; Wouters, H.; Cagno, S.; Janssens, K.; Terryn, H.; Nys, K.; Thienpont, H. Optical spectroscopy as a rapid and low-cost tool for the first-line analysis of glass artefacts: A step-by-step plan for Roman green glass. *J. Archaeol. Sci.* **2011**, *38*, 2387–2398. [CrossRef]
24. Rebollo, E.; Ratti, F.; Cortelazzo, G.M.; Poletto, L.; Bertoncello, R. New trends in imaging spectroscopy: The non-invasive study of the Scrovegni Chapel stained glass windows. In Proceedings of the O3A: Optics for Arts, Architecture, and Archaeology III, Munich, Germany, 25–26 May 2011; Volume 8084.
25. Palomar, T.; Grazia, C.; Cardoso, I.P.; Vilarigues, M.; Miliani, C.; Romani, A. Analysis of chromophores in stained-glass windows using Visible Hyperspectral Imaging in-situ. *Spectrochim. Acta Part A-Mol. Biomol. Spectrosc.* **2019**, *223*, 117378. [CrossRef] [PubMed]
26. Perri, A.; de Faria, B.E.N.; Ferreira, D.C.T.; Comelli, D.; Valentini, G.; Preda, F.; Polli, D.; de Paula, A.M.; Cerullo, G.; Manzoni, C. Hyperspectral imaging with a TWINS birefringent interferometer. *Opt. Express* **2019**, *27*, 15956–15967. [CrossRef] [PubMed]
27. Funatomi, T.; Ogawa, T.; Tanaka, K.; Kubo, H.; Caron, G.; Mouaddib, E.M.; Matsushita, Y.; Mukaigawa, Y. Eliminating Temporal Illumination Variations in Whisk-broom Hyperspectral Imaging. *Int. J. Comput. Vis.* **2022**, *130*, 1310–1324. [CrossRef]
28. Babini, A.; George, S.; Hardeberg, J.Y. *Hyperspectral Imaging Workflow for the Acquisition and Analysis of Stained-Glass Panels*; SPIE: Bellingham, WA, USA, 2021; Volume 11784.
29. *ISO 5-2*; Photography and Graphic Technology—Density Measurements: Part 2: Geometric Conditions for Transmittance Density. ISO: Geneva, Switzerland, 2009.
30. *CIE 15*; Technical Report: Colorimetry 3rd Edition. International Commission on Illumination: Vienna, Austria, 2004.
31. *ISO 13655*; Graphic Technology—Spectral Measurement and Colorimetric Computation for Graphic Arts Images. ISO: Geneva, Switzerland, 2017.
32. Pillay, R.; Hardeberg, J.Y.; George, S. Hyperspectral imaging of art: Acquisition and calibration workflows. *J. Am. Inst. Conserv.* **2019**, *58*, 3–15. [CrossRef]
33. Schindelin, J.; Arganda-Carreras, I.; Frise, E.; Kaynig, V.; Longair, M.; Pietzsch, T.; Preibisch, S.; Rueden, C.; Saalfeld, S.; Schmid, B.; et al. Fiji: An open-source platform for biological-image analysis. *Nat. Methods* **2012**, *9*, 676–682. [CrossRef]
34. IGT Testing Systems. IGT Reference Paper C2846. Available online: https://www.igt.nl/product/igt-reference-paper/ (accessed on 6 June 2022).
35. *ISO/TS 23031*; Graphic Technology—Assessment and Validation of the Performance of Spectrocolorimeters and Spectrodensitometers. ISO: Geneva, Switzerland, 2020.
36. Ohta, N.; Robertson, A.R. CIE Standard Colorimetric System. In *Colorimetry: Fundamentals and Applications*; John Wiley: Chichester, UK; Hoboken, NJ, USA, 2005.
37. Green, P.; MacDonald, L.W. *Colour Engineering: Achieving Device Independent Colour*; John Wiley and Sons: Chichester, UK, 2002.
38. Luo, M.R.; Cui, G.; Rigg, B. The development of the CIE 2000 colour-difference formula: CIEDE2000. *Color Res. Appl.* **2001**, *26*, 340–350. [CrossRef]
39. *ISO/CIE 11664-6*; Colorimetry—Part 6: CIEDE2000 Colour-Difference Formula. ISO: Geneva, Switzerland, 2014.
40. Ceglia, A.; Meulebroeck, W.; Wouters, H.; Baert, K.; Nys, K.; Terryn, H.; Thienpont, H. Using optical spectroscopy to characterize the material of a 16th c. stained glass window. In Proceedings of the Integrated Approaches to the Study of Historical Glass—Ias12, Brussels, Belgium, 16–17 April 2012; Volume 8422.
41. Ceglia, A.; Meulebroeck, W.; Cosyns, P.; Nys, K.; Terryn, H.; Thienpont, H. Colour and Chemistry of the Glass Finds in the Roman Villa of Treignes, Belgium. *Procedia Chem.* **2013**, *8*, 55–64. [CrossRef]
42. Green, L.R.; Alan Hart, F. Colour and chemical composition in ancient glass: An examination of some roman and wealden glass by means of ultraviolet-visible-infra-red spectrometry and electron microprobe analysis. *J. Archaeol. Sci.* **1987**, *14*, 271–282. [CrossRef]
43. Ceglia, A.; Meulebroeck, W.; Baert, K.; Wouters, H.; Nys, K.; Thienpont, H.; Terryn, H. Cobalt absorption bands for the differentiation of historical Na and Ca/K rich glass. *Surf. Interface Anal.* **2012**, *44*, 219–226. [CrossRef]
44. Farges, F.; Etcheverry, M.P.; Scheidegger, A.; Grolimund, D. Speciation and weathering of copper in "copper red ruby" medieval flashed glasses from the Tours cathedral (XIII century). *Appl. Geochem.* **2006**, *21*, 1715–1731. [CrossRef]
45. Colomban, P.; Tournie, A.; Ricciardi, P. Raman spectroscopy of copper nanoparticle-containing glass matrices: Ancient red stained-glass windows. *J. Raman Spectrosc.* **2009**, *40*, 1949–1955. [CrossRef]
46. Kunicki-Goldfinger, J.J.; Freestone, I.C.; McDonald, I.; Hobot, J.A.; Gilderdale-Scott, H.; Ayers, T. Technology, production and chronology of red window glass in the medieval period—Rediscovery of a lost technology. *J. Archaeol. Sci.* **2014**, *41*, 89–105. [CrossRef]

47. Manikandan, D.; Mohan, S.; Magudapathy, P.; Nair, K.G.M. Blue shift of plasmon resonance in Cu and Ag ion-exchanged and annealed soda-lime glass: An optical absorption study. *Phys. B Condens. Matter* **2003**, *325*, 86–91. [CrossRef]
48. Bacon, F.R.; BlLllAn, C.J. Color and Spectral Transmittance of Amber Bottle Glass. *J. Am. Ceram. Soc.* **1954**, *37*, 60–66. [CrossRef]
49. Capobianco, N.; Hunault, M.O.J.Y.; Loisel, C.; Trichereau, B.; Bauchau, F.; Trcera, N.; Galoisy, L.; Calas, G. The representation of skin colour in medieval stained glasses: The role of manganese. *J. Archaeol. Sci. Rep.* **2021**, *38*, 103082. [CrossRef]
50. Fernandes, P.; Vilarigues, M.; Alves, L.C.; da Silva, R.C. Stained glasses from Monastery of Batalha: Non-destructive characterisation of glasses and glass paintings. *J. Cult. Herit.* **2008**, *9*, e5–e9. [CrossRef]